LAWRENCE
LIVERMORE
NATIONAL
LABORATORY

LLNL-TR-401217

Residual stress measurement and microstructural characterization of thick beryllium films

A. Detor, M. Wang, A. M. Hodge, E. Chason, C. Walton, A. V. Hamza, H. Xu, A. Nikroo

February 11, 2008

Disclaimer

This work performed under the auspices of the U.S. Department of Energy by Lawrence Livermore National Laboratory under Contract DE-AC52-07NA27344.

Residual stress measurement and microstructural characterization of thick beryllium films

Andrew Detor [1], Morris Wang [1], Andrea Hodge [2], Eric Chason [3], Chris Walton [1], Alex Hamza [1], Hongwei Xu [4], Abbas Nikroo [4]

[1] Lawrence Livermore National Laboratory, Livermore, CA
[2] University of Southern California, Los Angeles, CA
[3] Brown University, Providence, RI
[4] General Atomics, San Diego, CA

Beryllium films are synthesized by a magnetron sputtering technique incorporating *in-situ* residual stress measurement. Monitoring the stress evolution in real time provides quantitative through-thickness information on the effects of various processing parameters, including sputtering gas pressure and substrate biasing. Specimens produced over a wide range of stress states are characterized via transmission and scanning electron microscopy, and atomic force microscopy, in order to correlate the stress data with microstructure. A columnar grain structure is observed for all specimens, and surface morphology is found to be strongly dependent on processing conditions. Analytical models of stress generation are reviewed and discussed in terms of the observed microstructure.

1. Introduction

As one of the lightest structural metals, beryllium is an ideal candidate material for inertial confinement fusion target applications. Over the past decade, much work has involved processing this material into small, ~1 mm diameter capsules as required to achieve ignition [1-5]. Of principal importance in this application is the ability to retain hydrogen gas at moderate pressures, which has perhaps been the greatest challenge to date. The problem is mainly a result of high residual stresses that develop during the synthesis of beryllium to the required thickness (~100 μm), which lead to cracking and porosity – fast paths for hydrogen diffusion.

To solve this problem, most of the previous work has been directed by an engineering approach, linking processing conditions to a qualitative evaluation of the final capsule and gas retention data. While this approach has led to some success, the present work seeks to investigate the stress generating mechanisms on a fundamental level. We incorporate novel *in-situ* stress measurements and detailed microstructural characterization with the goal of understanding and ultimately controlling residual stress. This "ground-up" approach has led to important scientific contributions in the field of thick film residual stress.

2. Experimental procedures

Beryllium films are deposited onto 25.4 mm diameter substrates using a magnetron sputtering technique at General Atomics (San Diego, CA). This technique is identical to that used for fusion target fabrication, with the exception that the substrates are flat in the present study. The stress developed during deposition is measured in real time using a multi-beam optical sensor (MOS) system manufactured by k-Space Associates, Inc. (Ann Arbor, MI) [6]. This system uses an array of parallel laser beams reflected from the surface during film growth to measure curvature, which is converted to stress using the Stoney formula [7]. These *in-situ* measurements allow for a detailed understanding of film stress evolution with thickness.

Following deposition, several techniques are used to characterize the film microstructure. A FEI Nova 600 scanning electron microscope (SEM) is used to image the surface morphology of as-

deposited films, and a Digital Instruments DIM-3000 atomic force microscope (AFM) allows for quantitative surface roughness measurements. Grain structure is evaluated in cross-section with a Philips CM300 transmission electron microscope (TEM) operating in bright-field mode; specimens for TEM are prepared using a focused ion beam (FIB) lift-out technique [8].

A number of processing variable have been considered to date, including: deposition flux, substrate material, substrate temperature, sputtering gas pressure, and substrate biasing. The latter two have been found to significantly affect the residual stress and microstructure; these variables will be the main focus of what follows. All experiments in the present work are conducted on Si<100> substrates initially at room temperature, using three magnetrons operating at 100 W each, under a background pressure of better than 8×10^{-6} mTorr.

3. Stress measurements

Experimental measurements of residual stress typically rely on *ex-situ* curvature measurements, which allow for an average film stress to be calculated. While this may be an acceptable measurement for thin films (<~100 nm), it can be misleading for thick depositions where significant gradients in residual stress are possible. In this case, a single average measurement may not fully characterize the stress state of the film. This problem is exemplified in Fig. 1, which plots the average stress in beryllium, at several film thicknesses from 0.5 to 2.0 μm, as a function of sputtering gas pressure. The general trend observed here for specimens deposited without substrate bias (circles) is consistent

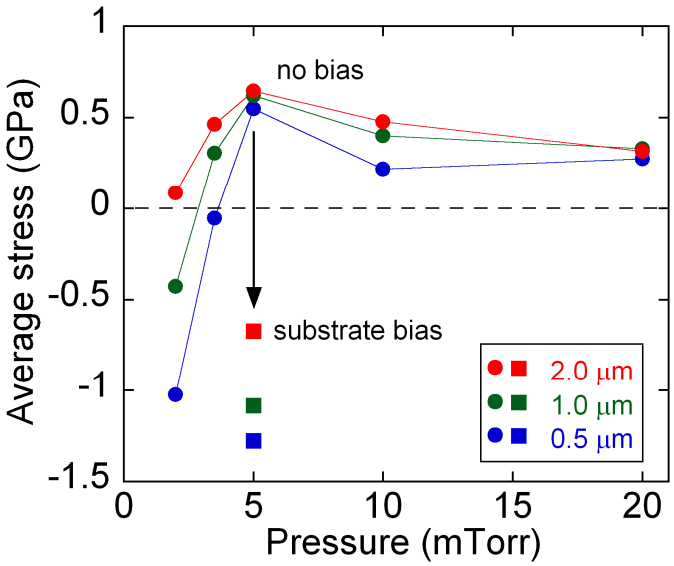

Figure 1: Average stress plotted as a function of sputtering gas pressure, measured at film thicknesses of 0.5, 1.0, and 2.0 μm. Note the general trend towards tensile stress as thickness increases. Results for a single specimen deposited at 5 mTorr under an applied substrate bias of -40 V are also shown for comparison

with a number of other systems in the literature [9-20]; compressive stress at low pressures, followed by a peak and eventual decline of tensile stress as pressure is increased (the reason for this trend will be discussed in detail in section 5). The main point here is that average stress changes with film thickness, generally trending in the tensile direction. Thus, stress is not constant through-thickness, but involves some more complicated behavior.

Also shown in Fig. 1 are average stress measurements for a specimen deposited with a -40 V bias applied to the substrate (square data points). This preliminary experiment shows that biasing can induce significant compressive stress in beryllium, which is again consistent with a number of observations in the literature for a variety of sputtered materials [16, 19-25]. Note, however, that the trend towards tensile stress remains as film thickness increases.

The observations above demonstrate a serious problem in using average stress to characterize thick films. As an alternative, we use the MOS system in the present work to measure stress as a function of thickness in real-time. In Fig. 2, "instantaneous" stress is plotted for a representative set of specimens from Fig. 1 encompassing a wide range of stress behavior. Instantaneous stress can be interpreted as the stress contributed to the specimen at a particular thickness, at or near the growing surface, during film growth. Integrating the results in Fig. 2 over thickness leads to the average measurements shown in Fig. 1; note the trend towards tensile stress for the lower two curves while the upper curve remains fairly flat. The main benefit of this instantaneous measurement lies in the spatial information; the results in Fig. 2 can be directly compared with the microstructure through-thickness. This enables unique comparison and insight on the stress generating mechanisms.

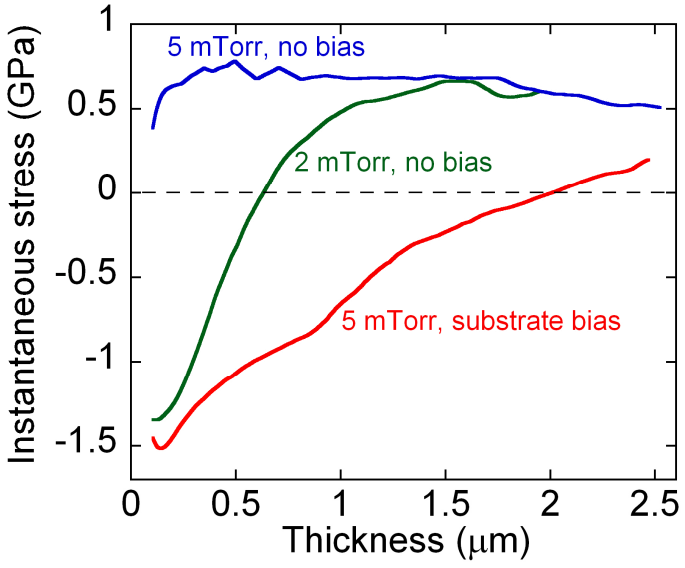

Figure 2: Instantaneous stress measured as a function of thickness using the MOS system. Three representative specimens are shown capturing a wide range of stress behavior. These spatial results can be directly compared to the microstructure through-thickness

4. Microstructure characterization

To interpret the results of Fig. 2, we now attempt to correlate the instantaneous stress with microstructural features. We begin with cross-sectional TEM experiments to characterize the grain structure, followed by an SEM examination of the final surface morphology, focusing on qualitative trends with processing conditions. We then characterize the surface structure quantitatively using AFM, paying special attention to surface roughness measurements.

Cross-sectional TEM images are shown in Fig. 3 (a-c) for the set of processing conditions in Fig. 2, arranged in order of increasing average compressive stress. Arrows indicate the direction of film growth and the entire thickness is captured in all cases, showing both the substrate interface and surface; in (a) the edge of the FIB lift-out specimen is also shown. Columnar growth is obvious in these images, regardless of processing conditions, with an area of dense nucleation near the substrate followed by well-defined grains oriented in the growth direction. The only notable difference is the slightly finer grain structure maintained in the biased condition (c), where the average grain size near the surface, ~80 nm, is roughly 40% less than that in (a) and (b). Otherwise, there is no clear correspondence between the grain structure in Fig. 3 (a-c) and the stress measurements in Fig. 2; no obvious trends in the microstructure can explain the stress evolution.

High-resolution surface SEM images are shown in Fig. 3 (d-f). Note that these images are taken after deposition is complete, representing the termination of the instantaneous stress curves in Fig. 2. The morphology of (d) and (e) appear similar, with nodular growth patterns that in some cases resemble the expected hexagonal shape for basal textured beryllium; this is especially apparent in (d). Both of these specimens are under nearly identical instantaneous stress levels at the thickness investigated (c.f. Fig. 2). The biased specimen in (f), on the other hand, shows very different surface morphology with a dense, well-defined grain structure. The instantaneous stress contributed by this surface is ~60 % less than that in (d) and (e). These observations suggest that the surface morphology may play an important role in determining the stress state. To investigate the surface

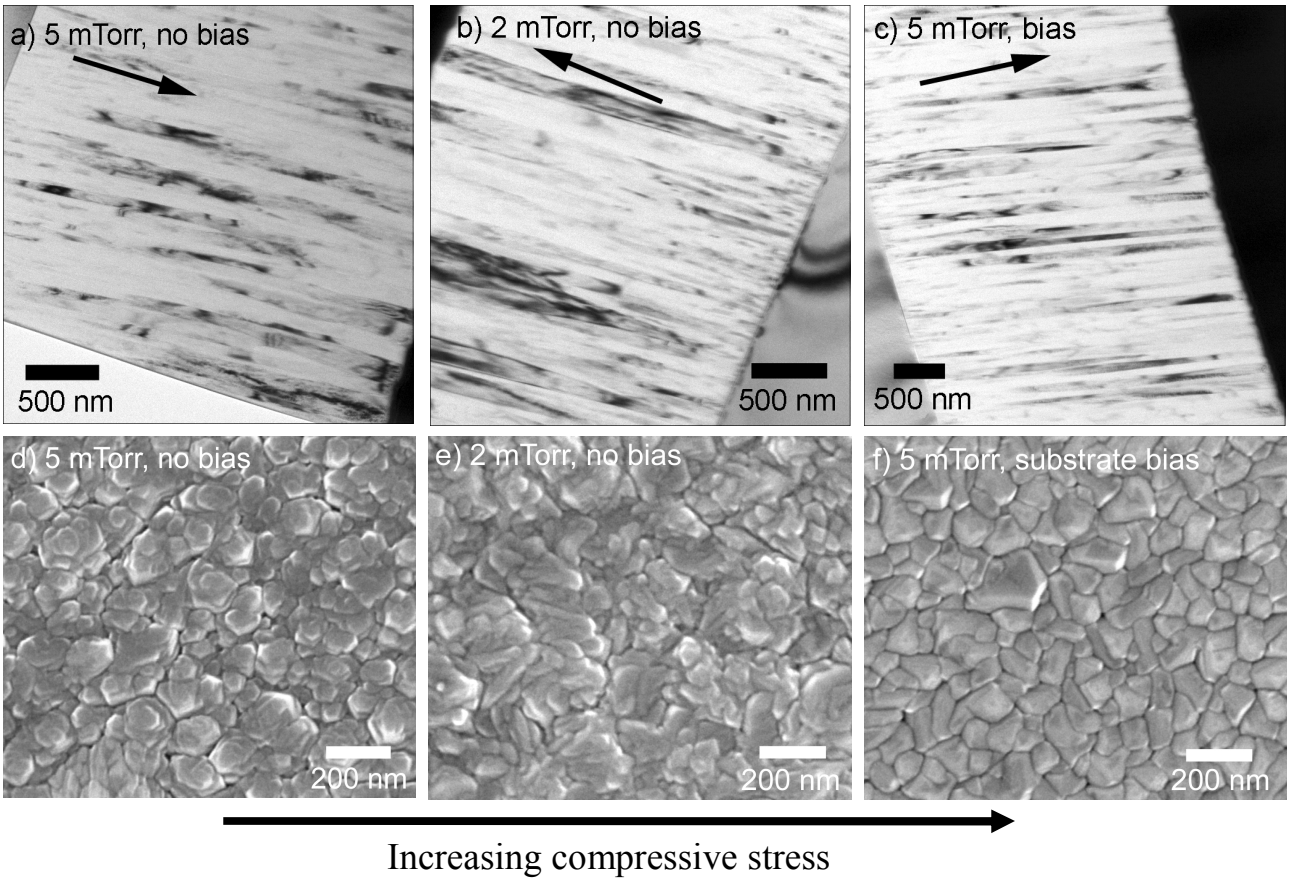

Figure 3: Bright-field TEM images of specimens deposited at (a) 5 and (b) 2 mTorr sputtering gas pressure without biasing, and (c) 5 mTorr with a -40V bias applied to the substrate, corresponding to the conditions in Fig. 2. Both the substrate interface and surface can be seen in these images; arrows indicate the approximate direction of film growth. (d), (e), and (f): surface SEM images of the specimens in (a), (b), and (c), respectively.

structure more quantitatively, AFM experiments are performed to measure RMS surface roughness; the specimens in (d), (e), and (f) yield values of 14.1, 15.4, and 9.9 nm, respectively. The scaling in surface roughness is similar to that for instantaneous stress with the smoother biased surface contributing less tensile stress. In the next section we consider several theoretical mechanisms proposed for stress generation in deposited films, with the goal of interpreting the above microstructural observations.

5. Comparison with analytical models

A number of models have been proposed to explain residual stresses developed during film deposition, and this remains an active area of research to date [26-40]. These models may be broadly classified into those that describe tensile or compressive stress generating mechanisms. In

this section we review several of the more popular models, focusing on specific variables that can be linked to the above microstructural observations.

a. Tensile stress

One of the first successful models of tensile stress generation was proposed by Hoffman [26], who considered the stress developed when newly deposited grains are attracted to one another during deposition, causing grain coalescence or "zipping" of the grain boundaries. This in-plane elastic strain produces a biaxial stress, σ_T, in the film which, to a first approximation, can be expressed as [26]:

$$\sigma_T = \frac{Y}{1-\nu} \cdot \frac{\Delta}{d} \tag{1}$$

where Y is Young's modulus, ν is Poisson's ratio, d is the grain size, and Δ is the critical gap over which neighboring grains are attracted to one another. Most tensile stress models in the literature are based on Eq. (1), aimed at deriving values for Δ based on energetic quantities (such as grain boundary and surface energies) [27], or incorporating modifications for specific geometries [33-35, 39, 40]. It is generally assumed that values of Δ are on the order of atomic dimensions, where attractive bonding forces can supply sufficient energy for spontaneous grain coalescence. Assuming typical values for beryllium [41] of Y=318 GPa, and ν=0.02, with a grain size of d=100 nm and Δ=0.2 nm, Eq. (1) yields a tensile stress of ~650 MPa, in line with the maximum experimentally observed in Fig. 2. Although this model is highly simplified, and dependent on the specific value of Δ, it provides a quantitative understanding of the potential mechanism and predicts reasonable stress levels. However, several other factors must be contributing to the stress data measured in Fig. 2, as Eq. (1) cannot fully describe the behavior. For instance, Eq. (1) predicts that tensile stress should decrease with increasing grain sizes, whereas we see the opposite effect. Also, there is an apparent plateau in the stress data at ~500 MPa, which is not incorporated in Eq. (1). This latter effect is likely due to the tensile strength of beryllium, which is at about the same level as the observed plateau [41] (i.e. the material simply cannot support higher levels of tensile

stress). For former, however, requires further explanation and may be linked to the surface morphology as discussed below.

As previously mentioned, a number of works have built on the simplicity of Eq. (1) to incorporate more complex growth behavior. Recently, researchers have focused on the effects of surface roughness, mainly through the aid of computational methods such as finite element analysis [33, 40]. One of the main outcomes of these works is a predicted correlation between surface roughness and tensile stress; rougher surfaces generate higher tensile stress due to the propensity for in-plane contact between neighboring grain surfaces. Although most of these works concentrate on thin films, it is well established that surface roughness generally increases during growth. Consequently, thicker films should be increasingly prone to tensile stress. This line of reasoning may explain the tensile trend with thickness in Figs. 1 and 2, and work is currently underway to investigate this effect in more detail, including both experimental and analytical efforts.

b. Compressive stress

Models of compressive stress have received comparatively less attention in the literature, primarily because most synthesis techniques and materials are more prone to tensile stress. Nevertheless, there have been several models proposed based on the idea of "atomic peening", similar to the macroscopic phenomena of shot peening, where the bombardment of high-energy atoms can induce compressive stress on the surface of a growing film [11, 28, 29, 31, 32]. Naturally, this mechanism only applies to energetic processing techniques, such as magnetron sputtering. A key requirement of these models is that the energy of incoming atoms, E, be greater than some critical value, E_{crit}, required to cause local atomic displacements (typically ~10-100 eV). For relatively low fluxes, the models of Windischmann [28] and Davis [29] yield similar results, predicting the level of compressive stress, σ_C, to be:

$$\sigma_C = \kappa \frac{Y}{1-\nu}\left[\frac{j \cdot E^{1/2}}{R}\right] \tag{2}$$

where R is the total flux of deposited atoms, j is the flux of energetic atoms arriving at the surface (with $E > E_{crit}$), and κ is a proportionality constant. Thus, high energy processing conditions will tend to yield compressively stressed films. This mechanism can be used to explain the stress results of the present work: low sputtering gas pressures lead to higher energy conditions and, hence, the transition to compressive stress below 5 mTorr in Fig. 1 (note that the lower apparent stresses above 5 mTorr is a processing artifact [11], related to higher levels of porosity in the film under these conditions). Similarly, biasing also leads to highly energetic conditions, yielding the most compressive stress of all experiments performed in the present work.

The total residual stress developed during deposition will involve some combination of the above mentioned mechanisms, and while it is highly unlikely that any one equation will precisely predict the stress level, these models provide some guidance on how to control and interpret experimental findings. High energy conditions, achieved through either low sputtering pressures or the application of substrate bias, tend to increase compressive stress. However, tensile stress is observed to increase to a material-dependent plateau with film growth, possibly owing to a change in surface morphology and the corresponding activation of grain coalescence mechanisms.

6. Conclusions

The present work has identified and explored two key processing variables affecting the stress state of sputter deposited beryllium: gas pressure and substrate biasing. We have shown that average stress measurements, while sufficient for thin films, do not fully characterize the complex stress state of thick deposits. Using the *in-situ* capabilities of the MOS system, film stress has been quantified as a function of thickness enabling detailed understanding of the stress evolution under various processing parameters with the following main conclusions:

- Regardless of processing conditions, instantaneous stress always tends in the tensile direction with film thickness.
- A maximum stress plateau is observed coinciding with the tensile strength of beryllium.

- Compressive stress can be induced during the early stages of film growth under high-energy deposition conditions, including the use of substrate biasing and/or low sputtering gas pressures.

In order to interpret the *in-situ* stress measurements from a microstructural standpoint, characterization has been performed via TEM, SEM, and AFM techniques. The main results can be summarized as follows:

- A clear columnar grain structure exists in all deposits; however, no clear relationship can be drawn between the structure and stress measurements.
- Surface morphology appears to be closely correlated with instantaneous stress; rougher surfaces leading to higher levels of tensile stress.

References

1. Chen, C.W. and Alford, C.S., J Vac Sci Tech A, **6**, 128-133, (1988).
2. McElfresh, M., et al., Fusion Sci Tech, **49**, 786-795, (2006).
3. Nikroo, A., et al., Phys Plasmas, **13**, 056302, (2006).
4. Nikroo, A., et al., Fusion Sci Tech, **51**, 553-558, (2007).
5. Xu, H.W., et al., Fusion Sci Tech, **51**, 547-552, (2007).
6. kSA Multi-beam optical sensor (MOS) system, k-Space Associates, Inc., www.k-space.com.
7. Stoney, G.G., Proc Royal Soc London A, **82**, 172-175, (1909).
8. Mayer, J., et al., MRS Bulletin, **32**, 400-407, (2007).
9. Thornton, J.A. and Hoffman, D.W., Thin Solid Films, **171**, 5-31, (1989).
10. Thornton, J.A. and Hoffman, D.W., J Vac Sci Tech, **14**, 164-168, (1977).
11. Windischmann, H., Crit Rev Solid State Mater Sci, **17**, 547-596, (1992).
12. Hoffman, D.W., J Vac Sci Tech A, **12**, 953-961, (1994).
13. Cuthrell, R.E., et al., J Vac Sci Tech A, **6**, 2914-2920, (1988).
14. Vink, T.J., et al., J Appl Phys, **74**, 988-995, (1993).
15. Vink, T.J., et al., J Appl Phys, **70**, 4301-4308, (1991).
16. Tranchant, J., et al., Surf Coat Tech, **200**, 6549-6553, (2006).
17. Shen, Y.G., et al., J Appl Phys, **87**, 177-187, (2000).
18. Shen, Y.G., Mater Sci Eng A, **359**, 158-167, (2003).
19. Misra, A. and Nastasi, M., J Mater Res, **14**, 4466-4469, (1999).
20. Andritschky, M. and Teixeira, V., Vacuum, **43**, 455-458, (1992).
21. Bielawski, M., Surf Coat Tech, **200**, 3987-3995, (2006).
22. Kim, S.P., Choi, H.M., and Choi, S.K., Thin Solid Films, **322**, 298-302, (1998).

23. Janssen, G.C.A.M. and Kamminga, J.D., Appl Phys Lett, **85**, 3086-3088, (2004).
24. Knoll, R.W. and Bradley, E.R., Thin Solid Films, **117**, 201-210, (1984).
25. Ljungcrantz, H., et al., J Appl Phys, **78**, 832-837, (1995).
26. Hoffman, R.W., Thin Solid Films, **34**, 185-190, (1976).
27. Nix, W.D. and Clemens, B.M., J Mater Res, **14**, 3467-3473, (1999).
28. Windischmann, H., J Appl Phys, **62**, 1800-1807, (1987).
29. Davis, C.A., Thin Solid Films, **226**, 30-34, (1993).
30. Knuyt, G., Thin Solid Films, **467**, 275-283, (2004).
31. Bilek, M.M.M. and McKenzie, D.R., Surf Coat Tech, **200**, 4345-4354, (2006).
32. Marks, N.A., McKenzie, D.R., and Pailthorpe, B.A., Phys Rev B, **53**, 4117-4124, (1996).
33. Seel, S.C. and Thompson, C.V., J Appl Phys, **93**, 9038-9042, (2003).
34. Sheldon, B.W., et al., J Appl Phys, **98**, 043509, (2005).
35. Sheldon, B.W., et al., Acta Mater, **55**, 4973-4982, (2007).
36. Rajamani, A., et al., Appl Phys Lett, **81**, 1204-1206, (2002).
37. Tello, J.S., et al., Phys Rev Lett, **98**, 216104, (2007).
38. Floro, J.A., et al., MRS Bulletin, **27**, 19-25, (2002).
39. Freund, L.B. and Chason, E., J Appl Phys, **89**, 4866-4873, (2001).
40. Sheldon, B.W., Lau, K.H.A., and Rajamani, A., J Appl Phys, **90**, 5097-5103, (2001).
41. Gale, W.F. and Totemeier, T.C., eds. *Smithells Metals Reference Book, 8th edition*. 2004, Elsevier Butterworth-Heinemann: Boston, MA.